

Investigation of vorticity production mechanisms in liquid atomization processes

Daniel Fuster, Maurice Rossi

▶ **To cite this version:**

Daniel Fuster, Maurice Rossi. Investigation of vorticity production mechanisms in liquid atomization processes. 29th Conference on Liquid Atomization and Spray Systems,, Oct 2021, paris, France. hal-03455903

HAL Id: hal-03455903
https://hal.science/hal-03455903

Submitted on 29 Nov 2021

HAL is a multi-disciplinary open access archive for the deposit and dissemination of scientific research documents, whether they are published or not. The documents may come from teaching and research institutions in France or abroad, or from public or private research centers.

L'archive ouverte pluridisciplinaire **HAL**, est destinée au dépôt et à la diffusion de documents scientifiques de niveau recherche, publiés ou non, émanant des établissements d'enseignement et de recherche français ou étrangers, des laboratoires publics ou privés.

Investigation of vorticity production mechanisms in liquid atomization processes

Daniel Fuster[1], Maurice Rossi[1]
[1]CNRS, Sorbonne Université, Institut Jean Le Rond d'Alembert, F-75005 Paris, France
*Corresponding author:fuster@dalembert.upmc.fr

Abstract
Atomization of a liquid jet is a challenge for Direct Numerical Simulation due to a wide range of length scales produced by the dynamics of interfaces. In this paper, we present the circulation production at an interface and its importance for energy dissipation. We point out the major role played by surface tension at interfaces on both production and dissipation. Evaluating numerically circulation production during liquid breakup is indeed critical to predict the vorticity generated in the overall atomization process. In order to shed light on the necessary conditions to resolve all scales in multiphase problems, we study the influence of surface tension, viscosity and grid resolution on two interface problems : the breakup of a liquid ligament by Rayleigh-Plateau instability and the liquid jet injection. Poorly resolved simulations generally tend to underestimate the total dissipation but in other cases, numerical discretization errors can lead to a large unphysical vorticity production overestimating the energy dissipation and deteriorating the quality of the numerical solution.

Keywords
Multiphase flow simulation, Surface tension effects, Energy dissipation.

Introduction

The simulation of atomization processes constitutes a challenging problem due to the difficulties to solve all scales in the flow. In single phase flows, it is typically assumed that unresolved structures act as an additional source of energy dissipation that can be modeled as an effective viscosity. In multiphase flow simulations, however, the role of unresolved scales on dissipation and large scale properties, is not yet completely understood.

In this work, we discuss the various sources of vorticity production related to the presence of an interface in a flow, and then focus our investigation on the effect of surface tension. Two multiphase flow problems are studied related to the fragmentation of a fluid into another fluid: the breakup of a ligament by a Rayleigh–Plateau instability and the atomization of a round jet in a stagnant fluid. We focus on surface tension effect by assuming negligible density and viscosity differences.

Numerical code

We use the Gerris Flow Solver [3] to solve the Navier–Stokes equations for a multiphase flow problem in the presence of surface tension. This solver is based on the Volume Of Fluid (VOF) method for interface tracking and it has implemented accurate and robust methods for surface tension forces. For the simulations, Adaptive Mesh Refinement (AMR) has been used based on both the color function and the vorticity field. Simulations are run with many processors through MPI parallelization. The code has been validated and widely used to investigate atomization processes [4].

Vorticity production and dissipation in a general multiphase flow problem

The generation of vorticity due to the presence of an interface can be understood by looking at the evolution of the circulation Γ of a closed curve $\mathbf{C}$ which crosses an interface S_{int} separating two phases. In two dimensions, the procedure used by [1, 2] yields

$$\frac{d}{dt}\Gamma = -\oint_{\mathbf{C}} [\nu \boldsymbol{\nabla} \times \boldsymbol{\omega}] \cdot \boldsymbol{t}\, \mathrm{d}\ell + \int_{I_f} S_\omega dl, \tag{1}$$

where the curve I_f is located on the interface S_{int} and connects the two intersections of curve $\mathbf{C}$ with the interface. The first integral is a classical diffusion term and the second integral corresponds to the vorticity sources located at the interface S_{int}. If velocity field is assumed continuous across the surface, quantity S_ω is

$$S_\omega = \frac{\partial}{\partial s}\left[\!\left[\frac{p}{\rho}\right]\!\right] = \left[\!\left[\frac{1}{\rho}\right]\!\right]\frac{\partial p_1}{\partial s} - \frac{1}{\rho_2}\frac{\partial}{\partial s}(\sigma\kappa) - \frac{2\,[\![\mu]\!]}{\rho_2}\frac{\partial^2}{\partial s^2}(\boldsymbol{u}\cdot\boldsymbol{t}). \tag{2}$$

where $[\![Q]\!] \equiv Q_1 - Q_2$ represents the jump of quantity Q between phases 1 and 2. This equation displays the importance of density differences, surface tension forces and viscous stresses on the production of vorticity across the interface. We extend this procedure in three dimensions with $[[\mu]] = 0$. This yields the same equation (1) with

This work is licensed under a Creative Commons 4.0 International License (CC BY-NC-ND 4.0).

the identical source (2) if one sets $[[\mu]] = 0$.

These three mechanisms (density differences, surface tension forces and viscous stresses) are also responsible for the overall energy dissipation. For a single fluid the dissipation can be written as a function of the vorticity and velocity fields as

$$\Phi = \mu\,\boldsymbol{\omega}^2 + 2\,\mu\,\boldsymbol{\nabla}\cdot\left[\boldsymbol{\omega}\times\boldsymbol{u} + \frac{1}{2}\,\boldsymbol{\nabla}(\boldsymbol{u}^2)\right]. \tag{3}$$

In order to investigate the impact of surface tension on energy dissipation we limit our studies in the present paper to situations where surface tension is the only physical effect generating vorticity at the interface i.e. we assume $[\![\mu]\!] = 0$ and $[\![\rho]\!] = 0$. In a domain bounded by solid walls, the total enstrophy $E = \int_V \boldsymbol{\omega}^2\,\mathrm{d}V$ is a direct measurement of dissipation

$$D = \int_V \Phi\,\mathrm{d}V = \mu E. \tag{4}$$

Results and discussion

Vorticity production during a ligament break-up.

First we consider the problem of liquid ligament of liquid 1 surrounded by a fluid 2. The interface characterized by a surface tension σ separates two fluids of identical density ρ and viscosity μ. At $t = 0$, both fluids are initially at rest and the interface is slightly deformed from a pure cylinder with an harmonic perturbation of wavelength L_0. Namely it is located at

$$R = R_0\,(1 + \epsilon\sin(kx))\,,\ \text{ with }\ k \equiv 2\pi/L_0,\quad \epsilon = 0.1 \tag{5}$$

If $kR_0 < 1$, the perturbation grows due to the Rayleigh–Plateau instability until pinch-off occurs. Otherwise the flow is stable and we only observe the damped oscillation of capillary waves. Note that an intrinsic length can be defined in this problem $\ell_\mu = \mu^2/(\sigma\rho)$.

Simulations are run in an axisymmetric configuration. We use a numerical square domain in the r, x plane of size L_0 to include one wavelength in the domain and a grid size Δ. Periodic boundary conditions are imposed at the right and left border and symmetric boundary conditions are applied at the top and bottom boundaries, that is $u_r = 0$, $\partial u_x/\partial r = 0$ and $\partial p/\partial r = 0$ at $r = 0$ and $r = L_0$. Taking as characteristic parameters of the problem radius R_0 and velocity $U_0 = \sqrt{\sigma/(R_0\rho)}$ based on fluid density and surface tension, the solution of the problem only depends on the dimensionless wavenumber of the perturbation, kR_0, and the Ohnesorge number $Oh = \mu/(\sqrt{\rho\sigma R_0})$ which plays the role of an inverse Reynolds number. Note that the intrinsic length $\ell_\mu = R_0 Oh^2$ increases with the Ohnesorge number Oh.

In the following, we investigate the influence of the Ohnesorge number and the dimensionless wavenumber kR_0 on the evolution in time of the kinetic energy $K = \rho/2\int_V \boldsymbol{u}^2\,\mathrm{d}V$, the enstrophy E and the maximum $D_{\max}$ over time of viscous dissipation over one wavelength. We will use as a matter of fact their rescaled counterparts K/K_0, E/E_0 and $D_{\max}/D_0$ with

$$K_0 \equiv \frac{M}{2}U_0^2,\quad E_0 \equiv V_0\frac{U_0}{R_0},\quad D_0 \equiv M\frac{U_0^3}{R_0}.$$

where $V_0 = \pi R_0^2 L_0$ and $M_0 = \rho V_0$ are the volume and mass of fluid 1 over one wavelength.This has to do with a sort of unit mass or unit volume quantity multiplied by the adequate product of large scale quantities U_0 and R_0.

First let us study the influence of grid size Δ on the results for $Oh = 2.2\cdot 10^{-2}$ and $Oh = 2.2\cdot 10^{-3}$ for a fixed wavenumber $kR_0 = 0.628$ which is located near the most unstable wavenumber of the Rayleigh–Plateau instability for a liquid jet ($kR_0 = 0.697$). Figures 1–2 show the evolution of the rescaled enstrophy E/E_0 and kinetic energy K/K_0 for various Δ/ℓ_μ. While the rescaled kinetic energy K/K_0 converges in both examples, rescaled enstrophy E/E_0 only convergences for the higher value $Oh = 2.2\cdot 10^{-2}$. This is consistent with the fact that the length ℓ_μ is larger in that case and it becomes easier to reach convergence. In addition, it appears on figures 1–2 that under–resolved simulations tend to under–predict the total dissipation rate as expected. Note that the maximum of enstrophy is reached after pinch-off during the retraction of the liquid bridge generating a satellite drop (figure 1 right).

We also study the influence of the Ohnesorge number on the convergence properties of the rescaled maximum of dissipation $D_{\max}/D_0$ when pinch-off occurs. This is shown in figure 3 for wavelength $kR_0 = 0.628$. The grid size conditions required for converged results seems to be $\Delta \le \min(100\ell_\mu, 0.5R_0)$. Remarkably, the converged value of $D_{\max}/D_0$ does not to depend significantly on Oh for sufficiently small values of $Oh < 0.1$. Figure 4 indicates that such conclusions hold irrespective of the value of the wavenumber in the regimes where pinch-off occurs ($kR_0 < 1$). Figure 5 depicts the results of the convergence study when the Rayleigh-Plateau instability is stable, $kR_0 = 1.256 > 1$. Compared to the pinch-off case ($kR_0 < 1$), the converged value of $D_{\max}/D_0$ is significantly lower

This work is licensed under a Creative Commons 4.0 International License (CC BY-NC-ND 4.0).

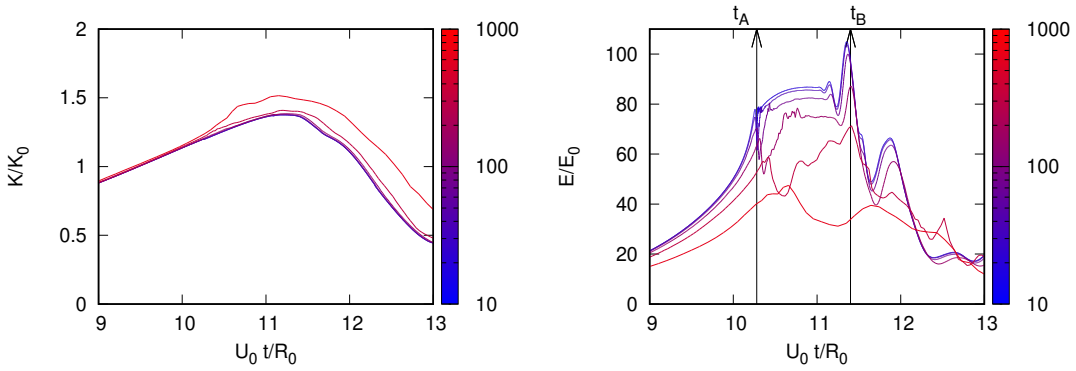


Figure 1. Temporal evolution during the pinch-off of a ligament of the rescaled kinetic energy K/K_0 (left) and the rescaled enstrophy E/E_0 (right) as a function of rescaled time $U_0 t/R_0$. The perturbation wavelength is $kR_0 = 0.628$ and $Oh = 2.2\,10^{-2}$. The color code ruler indicates the value of Δ/ℓ_μ. t_A denotes the instant at which pinch-off occurs and t_B is the instant where the ligament is retracted.

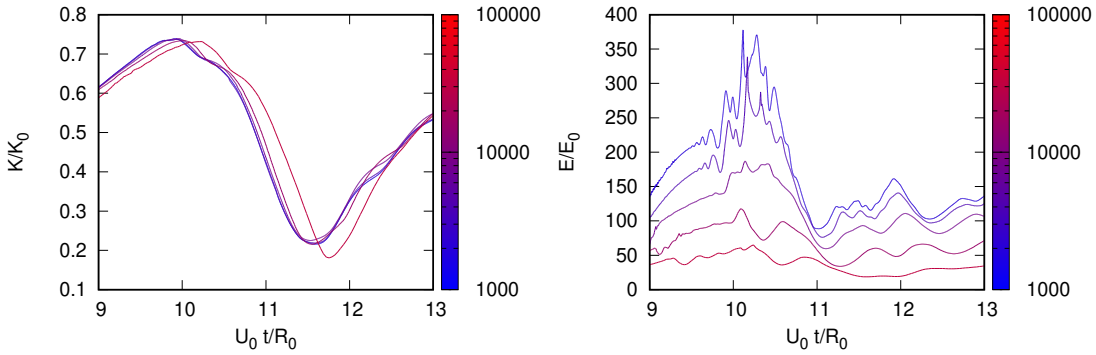


Figure 2. Temporal evolution during the pinch-off of a ligament of the rescaled kinetic energy K/K_0 (left) and the rescaled enstrophy E/E_0 (right) as a function of rescaled time $U_0 t/R_0$. The perturbation wavelength is $kR_0 = 0.628$ and $Oh = 2.2\,10^{-3}$. The color code ruler indicates the value of Δ/ℓ_μ.

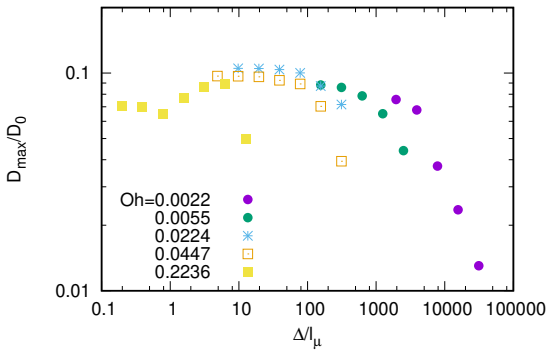


Figure 3. Influence of Oh for wavelength $kR_0 = 0.628$ on $D_{\max}/D_0$ the rescaled maximum of dissipation during the pinch-off process of a ligament as a function of Δ/ℓ_μ

This work is licensed under a Creative Commons 4.0 International License (CC BY-NC-ND 4.0).

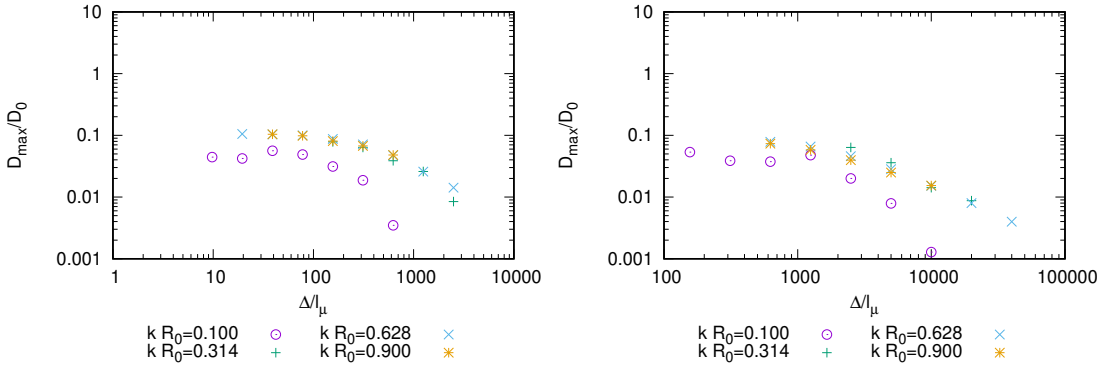


Figure 4. Influence of wavenumber kR_0 on the convergence of the rescaled maximum of dissipation $D_{\max}/D_0$ during the pinch-off. Four different wavenumbers are shown for the Ohnesorge number $Oh = 2.2\,10^{-2}$ (left) and $Oh = 5\,10^{-3}$ (right).

and depends as well on the Ohnesorge number. In this capillary regime, we expect the accuracy of results to be controlled by parameter $k\Delta$ rather than by the characteristic length ℓ_μ. Let us also pinpoint the sudden increase of dissipation at low resolutions $\Delta \approx R_0$. This increase is related to the ligament fragmentation by numerical method, in particular by the combined errors in interface reconstruction and curvature estimation, leading to significant errors in terms of enstrophy production and energy dissipation. This will be shown in more detail at the end of the next section.

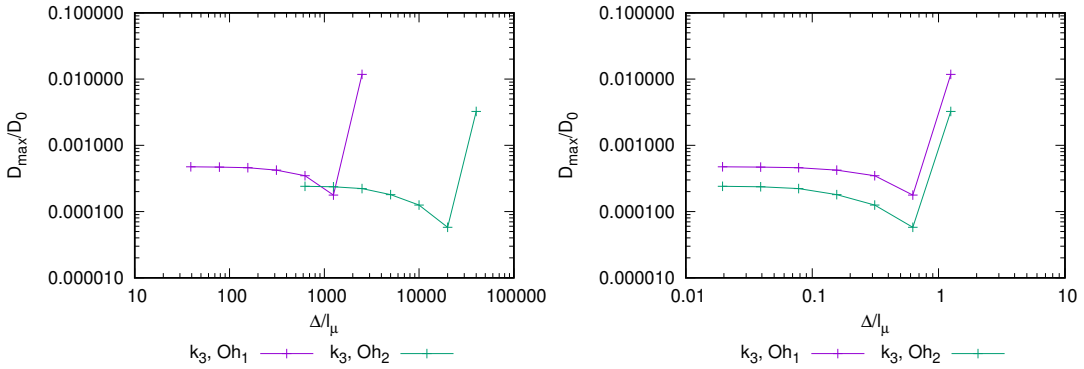


Figure 5. Convergence study of the rescaled maximum of dissipation $D_{\max}/D_0$ for the oscillation of capillary waves ($k_3 R_0 = 1.256$) for two different values of the Ohnesorge number: $Oh_1 = 2.2\,10^{-2}$, $Oh_2 = 5\,10^{-3}$

The liquid jet injection problem.

The second multiphase problem is the formation of a vortex ring by ejecting a fluid 1 outside an axisymmetric nozzle of radius R_0 at velocity U_0 in a semi-infinite domain initially at rest and filled with fluid 2. The two fluids share the same density ρ and viscosity μ but are immiscible and separated by an interface of surface tension σ. On the nozzle plate and on the left wall of the domain no-slip condition is enforced. The numerical domain is defined by a box of size $x \in [-2R_0, 34R_0]$ and $r \in [0, 17R_0]$. At the right boundary $x = 34R_0$, outflow conditions are imposed. Finally, at the exit of the nozzle $x = 0$, a Dirichlet boundary condition mimics the generation of an exiting jet : the velocity field is set to

$$\begin{cases} u_x(x=0,r,t) = U_0 \mathrm{erf}(t/\tau)\mathrm{erf}(\eta), \\ u_r(x=0,r,t) = 0 \quad \text{with } \eta = \dfrac{R_0 - r}{\sqrt{2}\,\delta_0}, \qquad \text{and } R_0 - r \geq 0 \end{cases} \tag{6}$$

For the examples considered here, the time $\tau = 0.05R_0/U_0$ is small compared to the characteristic time R_0/U_0 and the boundary layer thickness $\delta_0 = 0.05R_0$ is small compared to the characteristic radius R_0. This flow is defined by a *Reynolds* and a *Weber* number

$$Re = U_0 R_0/\nu, \quad We = \frac{\rho U_0^2 R_0}{\sigma}.$$

Figure 6 shows the results obtained for $Re = 1000$ and variable Weber We i.e. '$We = \infty, 1000, 100, 10$. For $We = \infty$, the classical problem of vortex formation is reproduced where the interface acts as a passive tracer that indefinitely rolls around the vortex creating very thin ligaments. When the surface tension takes low values

This work is licensed under a Creative Commons 4.0 International License (CC BY-NC-ND 4.0).

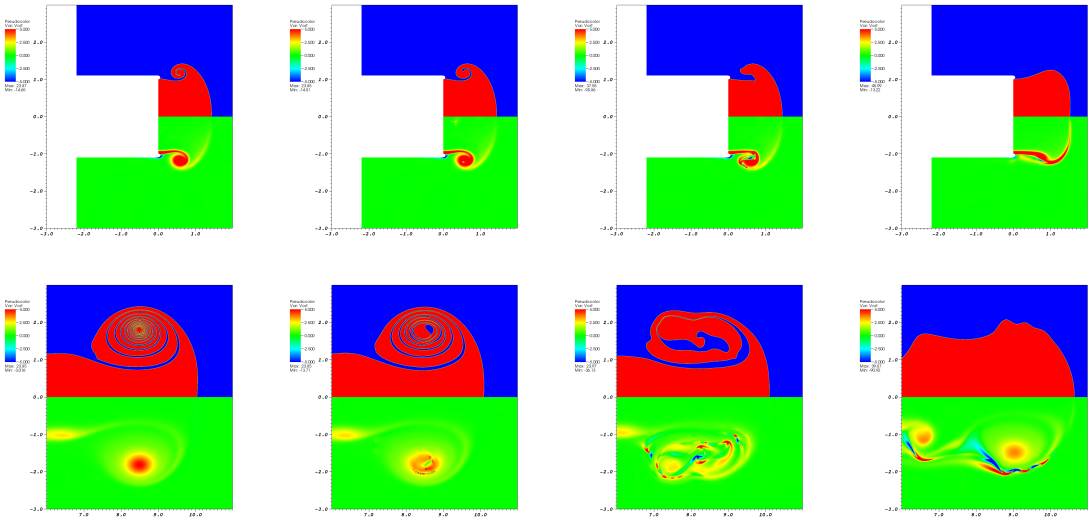


Figure 6. Simulations of liquid injection with an interface at $t = 2R_0/U_0$ (top) and $t = 20R_0/U_0$ (bottom). From left to right We=$\infty, 1000, 100, 10$.

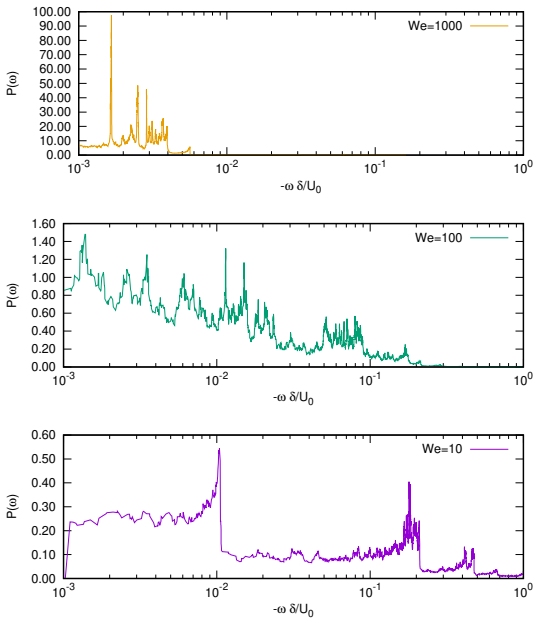


Figure 7. Probability density functions for negative vorticity contained at the interface at $t = 20R_0/U_0$ (snapshots shown in Figure 6). From top to bottom, the Weber number is equal to $\infty, 1000, 100, 10$. $Re = 1000$.

This work is licensed under a Creative Commons 4.0 International License (CC BY-NC-ND 4.0).

($We = 1000$), small fluctuations in the vorticity field appear but the structure of the vortex ring can be still clearly identified. In such a case, a rim appears at the tip of the ligament that prevents the interface from further rolling-up inside the core. The structure of the interface far from the vortex core however is similar to that observed for $We = \infty$. For $We = 100$ surface tension forces have a major influence on the topological evolution of the interface and on the vorticity field. The production of vorticity becomes clear in all regions where the interface is present and it is no longer possible to distinguish the clear presence of the vortex ring as in the case of $We = \infty$. Finally for $We = 10$, surface tension forces become more important than inertial forces: the interface does not roll any longer and the vortex ring generated is trapped inside the injected fluid. We can still see regions of significant vorticity production at the interface, especially in the regions of large curvature. In order to characterize the vorticity fields in Figure 6, we define a the cumulative function $C(\omega)$ as the probability within the interface region where vorticity is negative, to find a vorticity larger than $\omega < 0$. The numerical derivative with respect to ω is the probability density function $P(\omega) = dC/d\omega$ within the set of negative values of vorticity at the interface. Our analysis is restricted to negative vorticity since the regions of negative vorticity at the interface are directly related to the influence of surface tension, contrary to positive vorticity which are also present in the boundary layer at inflow. Figure 7 displays a significant influence of surface tension on the negative vorticity distributions at the interface. The values of negative vorticity shifts towards larger negative values as the Weber number decreases revealing that the intensity of the vorticity source due to the presence of the interface significantly increases as the Weber number decreases. In addition we observe the appearance of clear peaks at low Weber numbers associated to the presence of boundary layers appearing as a consequence of the combined effect of the interface topology and surface tension.

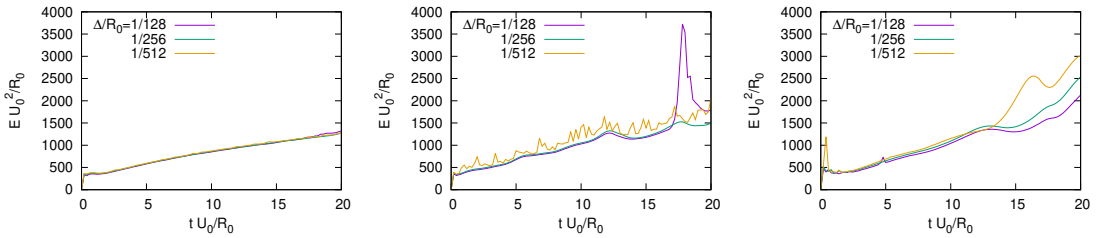


Figure 8. Temporal evolution of the rescaled enstrophy E/E_0 for three different Weber. From left to right: $We = 1000, 100, 10$ and $Re = 1000$.

In order to characterize the flow evolution in time, we use the enstrophy E and maximum over time of the viscous dissipation $D_{\max}$ in the numerical domain. More precisely we use their rescaled counterparts E/E_0 and $D_{\max}/D_0$ with $E_0 \equiv V_0 U_0/R_0$, $D_0 \equiv MU_0^3/R_0$ where $V_0 = \pi R_0^3$ and $M_0 = \rho V_0$ are the volume and mass contained in a cylinder of length R_0 and radius R_0 of fluid 1. Figure 8 shows the temporal evolution of E/E_0 for the three different cases in presence of surface tension and three different grid sizes. It is worth mentioning that, in the context of liquid atomization, numerical simulations reported in [5] have shown the difficulties to converge on the enstrophy production even for extremely refined grids. In the present case, surface tension has an important effect on the vorticity generated at the interface and therefore the amount of energy dissipated. For $We = 1000$, results are almost grid independent given that the vorticity generated at the interface is negligible compared to that of the vortex naturally formed from the roll-up of vorticity injected through the boundary layer present in the inlet boundary condition.

In the limit of small Weber numbers (here $We = 10$), it is more difficult to get convergence on the enstrophy generated by the interface, especially at large times, As previously, the total dissipation tends to increase as we refine the grid. Based on the results presented above, the difficulties to reach convergence are attributed to temporal discretization errors on the integration of the interface position in time.

At the intermediate Weber numbers (here green curves at $We = 100$), the situation is more challenging. Peaks of enstrophy during time evolution are strongly dependent on the grid size and their appearance is directly related to the breakup of thin ligaments (see Figure 9). This is consistent with the results reported in the previous section where we observe a sudden increase on the enstrophy production for very low resolutions. We note that even when the breakup is numerical, both positive and negative vorticity is generated which quickly diffuses and cancels out recovering an enstrophy level similar of the more refined grid where no fragmentation occurs.

Conclusions

In a general multiphase flow problem, surface tension and viscosity as well as density differences are the three main parameters influencing the amount of vorticity production and energy dissipation additionally created compared to that of a single phase flow. We focused on two problems where surface tension is the only mechanism responsible for vorticity production.

Results for the three-dimensional pinch-off of a liquid ligament indicates that it is possible to reach convergence for the energy dissipation despite the appearance of a singularity. For those situations where $\min(100\ell_\mu, 0.5R_0) <$

This work is licensed under a Creative Commons 4.0 International License (CC BY-NC-ND 4.0).

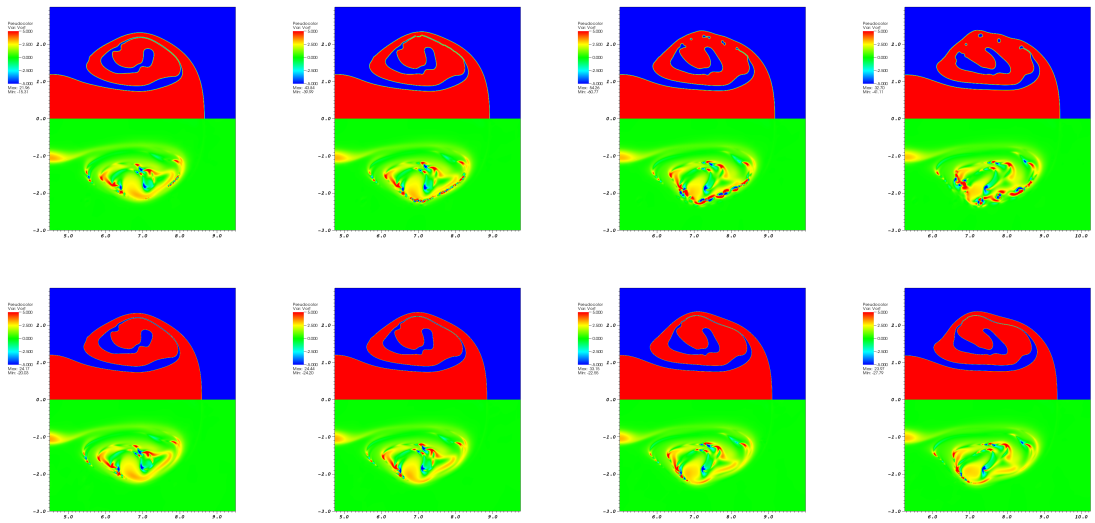


Figure 9. Interface and vorticity for $We = 100$ at times $tU_0/R_0 = 17.0, 17.5, 18.0, 18.5$. (top) Grid resolution $\Delta/R_0 = 7.8 \cdot 10^{-3}$ and (bottom) grid resolution $\Delta/R_0 = 3.9 \cdot 10^{-3}$.

$\Delta \ll R_0$ the amount of energy dissipated during the process of fragmentation is under–predicted. Finally, the case of $\Delta \gtrapprox R_0$ is shown to induce large errors on the enstrophy production, especially in those cases where no fragmentation should occur.

The injection of a round jet in a stagnant fluid in the presence of surface tension shows the promotion of vorticity production by surface tension forces and the appearance of different regimes of interaction between a vortex and an interface. From the perspective of the numerical simulation of the process the more challenging situations are found for intermediate values of the Weber number ($We = 100$) where the surface tension forces are sufficiently strong to generate a significant amout of vorticity but not intense enough to prevent the appearance of small scale structures appearing as a consequence of inertial effects. In this regime the breakup of thin ligaments due to the limited resolution lead to the appearance of enstrophy peaks that strongly depend on the grid size.

References

[1] T. Lundgren and P. Koumoutsakos. On the generation of vorticity at a free surface. *Journal of Fluid Mechanics*, 382:351–366, 1999.

[2] M. Brøns, M.C. Thompson, T. Leweke, and K. Hourigan. Vorticity generation and conservation for two-dimensional interfaces and boundaries. *Journal of Fluid Mechanics*, 758:63–93, 2014.

[3] S. Popinet. An accurate adaptive solver for surface-tension-driven interfacial flows *Journal of Computational Physics*, 228:5838–5866, 2009.

[4] D. Fuster, J.P. Matas, S. Marty, S. Popinet, J. Hoepffner, A. Cartellier, S. Zaleski. Instability regimes in the primary breakup region of planar coflowing sheets *Journal of Fluid Mechanics*, 736:150–176, 2013.

[5] Y.Ling, D. Fuster, G. Tryggvason, S. Zaleski. A two-phase mixing layer between parallel gas and liquid streams: multiphase turbulence statistics and influence of interfacial instability. *Journal of Fluid Mechanics*, 859:267–307, 2019.

This work is licensed under a Creative Commons 4.0 International License (CC BY-NC-ND 4.0).